Journal of Photochemistry & Photobiology, B: Biology 265 (2025) 113134

Contents lists available at ScienceDirect

Journal of Photochemistry & Photobiology, B: Biology

journal homepage: www.elsevier.com/locate/jphotobiol

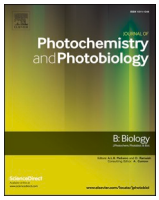

Photophysics of 5,6,7,8-tetrahydrobiopterin on a femtosecond time-scale

Varvara G. Kubenko, Vladimir A. Pomogaev, Andrey A. Buglak *, Alexei I. Kononov

St. Petersburg State University, Universitetskaya emb. 7-9, 199034, Saint-Petersburg, Russia

A R T I C L E I N F O

Keywords:
Pterins
Tetrahydrobiopterin
DFT
Multireference spin-flip (MRSF)
Fluorescence upconversion

A B S T R A C T

Pterins are naturally occurring compounds widespread in living organisms. 5,6,7,8-Tetrahydrobiopterin (H_4Bip) is a cofactor of several key enzymes, including NO-synthases and phenylalanine hydroxylase, whereas tetrahydrocyanopterin is a photoreceptor molecule in cyanobacteria. In this regard, tetrahydropterins (H_4pterins) photochemistry and photophysics have been attracting our attention. H_4pterins photodegrade in presence of molecular oxygen yielding dihydropterins (H_2pterins) and oxidized pterins. Meanwhile, the excited states dynamics of H_4pterins on a femto- and picosecond time-scale remains unclear. To shed light on this area, we perform time-resolved spectroscopy of H_4Bip using fluorescence up-conversion as well as transient absorption spectroscopy techniques along with TD-DFT non-adiabatic molecular dynamics. We show that the lowest H_4Bip exited state has a lifetime of ca. 200 fs. Using the BHandHLYP functional and multireference spin-flip (MRSF) method we demonstrate that starting from the S_4 state, H_4Bip passes to the S_1 state within 50 fs, and after 200 fs a conical intersection with the ground S_0 state is achieved. As a whole, the excited state behavior of H_4Bip is similar to DNA nucleobases, in particular guanine. These findings allow us to make some speculations about the biochemical role of H_4pterins photophysics.

1. Introduction

Pterins are naturally occurring compounds. Typically, they have three redox states (H_4pterins, H_2pterins and oxidized pterins) which are accompanied by free radical species [1]. H_4Pterins are widely-distributed as coenzymes in biological systems. Probably, the most well-known of them is 5,6,7,8-tetrahydrobiopterin (H_4Bip). H_4Bip acts a coenzyme of phenylalanine hydroxylase, alkylglycerol monooxygenase as well as NO-synthases [2]. H_4Bip is both pro- and antioxidant depending on molecular environment and conditions. Its biochemistry and biophysics is of great interest in recent studies [3–8].

In the last few years, H_4pterins (Fig. 1) attracted attention as photoactive compounds. Thus, oxidized pterins are often effective photosensitizers able to produce singlet molecular oxygen [9,10] whereas the main type of photosensitized reactions occur according to type I mechanism [11–13]. Multiple proteins exist as H_4Bip-dependent enzymes. For example, tyrosinase is inhibited by the excessive amount of H_4Bip [14]. Thus, oxidation of H_4Bip can activate the reactions catalyzed by the tyrosinase; therefore, the photo-oxidation of H_4Bip with participation of UV-B can affect melanogenesis [15].

H_4pterins are able to serve as photoreceptors/photoprotectors since their excited states is known to dissipate on a femtosecond timescale [1,16]. In particular, Moon and co-authors demonstrated that H_4cyanopterin (a glycosylated version of 6-substituted H_4pterin) is able to modulate the photo-movement of cyanobacteria in response to UV irradiation [17,18]. Cyanopterin-containing photoreceptor inhibits negative phototaxis induced by UV and blue light [17]. Photooxidation of H_4cyanopterin should affect photoreception of UVA by cyanobacteria [18]. Moreover, Takeda et al. showed that H_4Bip participates in UVB photoreception in higher plants [19].

The photooxidation of H_4Bip occurs through photosensitization mechanisms with participation of its degradation products: biopterin, pterin, carboxypterin, etc. Photooxidation is determined by multiple factors: solvent, molecular oxygen presence and character of UV irradiation. At the first stage, H_4Bip produces H_2pterins: quinonoid-6,7-H_2biopterin (qH_2Bip), 7,8-H_2Bip, 7,8-H_2Ptr, 7,8-H_2xanthopterin (Fig. 2) [20,21], etc.; whereas at the second stage, H_2pterins are degraded into oxidized pterins: pterin, biopterin, carboxypterin, formylpterin [22], etc. H_2pterins are also oxidized by reaction with dissolved oxygen [23] and by reactive oxygen species [24]. However, there is an alternative pathway to H_4Bip phototransformation, which is a dimerization of H_2Ptr and H_2Bip into $(H_2Ptr)_2$ and $(H_2Bip)_2$, respectively [25].

In this regard, we investigated the photophysics of 6-substituted H_4pterin using both experiment and theory. We established similar

* Corresponding author.
E-mail address: andreybuglak@gmail.com (A.A. Buglak).

https://doi.org/10.1016/j.jphotobiol.2025.113134
Received 18 October 2024; Received in revised form 18 February 2025; Accepted 20 February 2025
Available online 21 February 2025

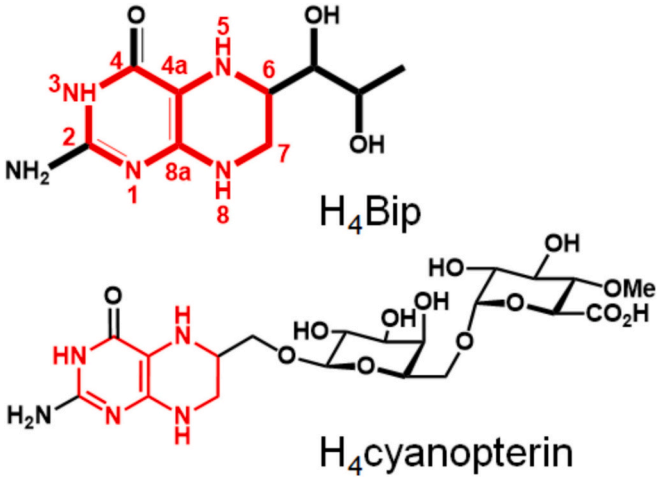

Fig. 1. Chemical formulas of H_4biopterin and H_4cyanopterin.

photophysics of H_4pterin and guanine within ultra-fast excited state internal conversion, which results in similar excited state lifetime of 0.5–1 ps [16]. Moreover, low ionization potential (ca. 7 eV) makes H_4pterin an effective antioxidant. Apparently, this set of properties could make H_4cyanopterin an effective photoreceptor of cyanobacteria [1]: apparently, for this reason, the concentration of H_4cyanopterin is nearly equal to chlorophyll *a* in modern cyanobacteria [26].

It is well known that the ultrafast internal conversion usually occurs through the conical intersections [27]. This theory for H_4pterins has been already developed by us in a recent paper [16]. Conical intersection (CoIn) is not only for ultrafast transitions, but is a model of electronic transitions in general. Searching for these points is determining energy barriers and structural deformation in excited states prepared for transitions. Dynamics should determine the lifetime of excited states before the transition, and this is, in principle, a statistical value.

Along the experimental data, conventional Time-Dependent Density Functional Theory (TDDFT) is used for structural optimization and calculation of vertical electron excitations (VEE), in particular, to generate static electronic absorption and emission spectra whereas the multiconfigurational linear response (LR) mixed-reference spin-flip (MRSF) approach based on TDDFT is applied for conical intersection (CoIn) searching between molecular excited electronic states with nonadiabatic molecular dynamics (NAMD) simulations, including the excited state energy dissipation, lifetimes of excited states, and probabilities of electronic transitions [28,29]. Multiconfigurational approaches enable the estimation of photochemical reactions [30,31] on photodynamic trajectories propagated by hybrid multilevel quantum-classical theories. Mixed reference spin flip (MRSF) demonstrates satisfactory accuracy [32–34] and requires significantly less computational resources compared to other QM/MD approaches. The hybrid quantum-classical molecular approach incorporates electronic quantum effects through gradients and embedding electrostatic potential fitting (ESPF) charges [34–36].

The present research provides a comprehensive analysis of photo-induced processes in a H_4pterin chromophore. Conventional TD-DFT is used for generating static electronic absorption and emission spectra, while MRSF is employed for propagating NAMD trajectories to study the dissipation of excited energies and to search for CoIn between molecular electronic states. Multiconfigurational methods are often needed to study excited state dynamics, in particular, excited state behavior is depicted by multiconfigurational methods in proximity of conical intersections. In general, TDDFT does not work in either CoIn or NAMD, there will be simply no transition between the states, only multi-configuration methods allow such transitions due to the mixing of states. Multiconfiguration methods are required for a reliable description of the conical intersections. MRSF is based on the initial calculation of the triplet in TDDFT, but uses it as the basic state to which all calculated singlets belong. MRSF was utilized to increase cost-effectiveness in light of the poor scaling of multiconfigurational methods [32–34].

The aim of this work was to study the dynamics of electronically excited states of H_4Bip. In order to achieve this purpose, the following tasks were addressed: 1) recording of spectral characteristics (absorption and steady-state luminescence spectra) under optimal conditions; 2) registration of luminescence kinetics and kinetics of photoinduced absorption; 3) simulation of H_4Bip excited states behavior using the MRSF method.

2. Materials and methods

2.1. Materials

(6*R*)-5,6,7,8-tetrahydro-L-biopterin was purchased from Schirks Laboratories (Switzerland). Phosphate buffer was of commercial origin (Sigma-Aldrich), whereas water was used from the Milli-Q purification system.

Immediately before sample preparation, the solvents were bubbled with nitrogen for one hour to remove dissolved oxygen. The samples were prepared and poured into a sealed cuvette in a nitrogen atmosphere box with an oxygen content of 0.1 %.

2.2. Absorption and steady-state luminescence spectroscopy

Absorption spectra were recorded using a Specord 210 Plus spectrophotometer (Analitik Jena) with a spectral slit width of 1 nm. Steady-state fluorescence spectra were obtained on a RF-6000 spectrofluorimeter (Shimadzu). The spectral widths of the slits in the excitation and emission channels were 5 nm. All measurements were performed at room temperature (22 ± 1 °C).

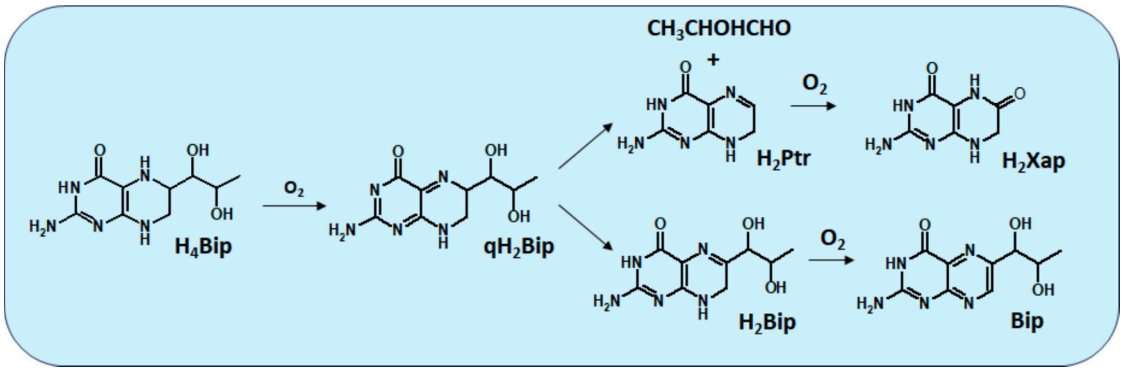

Fig. 2. Scheme of H_4Bip oxidation in an aqueous solution in presence of molecular oxygen [21].

2.3. Time-resolved spectroscopy

Time resolved experiments were performed in the absence of oxygen, as mentioned above in 2.1. A femtosecond laser complex was used to study ultrafast processes of H_4Bip. It consists of a regenerative amplifier Astrella V-USP-1 K (Coherent) on a titanium-sapphire crystal with a wavelength of 800 nm, a pulse duration of 40 fs, a pulse frequency of 1 kHz and an output power of 7 W, an optical parametric amplifier TOPAS-PrimeFP+NRV_MW with an average output power of 5 mW at the excitation wavelength of 270 nm, and two independent installations: a fluorescence up-conversion spectrometer FOG-100DA (CDP, Russia) – for measuring the kinetics of fluorescence by nonlinear total frequency generation with a time resolution better than 100 fs, and a pump-probe spectrometer ExciPro-XL (CDP, Russia) for measuring light-induced absorption changes with the pump-probe method. The measurements were performed in a round rotating 0.4 mm quartz cell. The concentration of H_4Bip was 3 mM (pH 7.5). The optical density was about 1. Decay curves were analyzed using DecayFit software.

When measuring fluorescence kinetics using a FOG100-DA spectrometer, the sample fluorescence is initiated by a femtosecond pump pulse and then directed to a nonlinear crystal where it is spatially combined with a gate pulse. Radiation at the sum frequency is generated only when the gate pulse coincides with a certain part of the fluorescence in time. Next, the photons are recorded using the PMT. The up-conversion signal is proportional to the fluorescence signal. By scanning the optical delay of the gate pulse relative to the pump pulse, the fluorescence kinetics are measured. The delay time is controlled by the delay line.

The optical scheme of FOG-100DA is shown in Fig. 3. The gate pulse (800 nm) is directed through diaphragms A1 and A2 to a corner reflector R installed on the optical delay line. Mirrors M1 and M2 direct the gate pulse to the nonlinear crystal, and lens L1 focuses it. The pump pulse (270 nm) is directed by mirrors M3, M4 and focusing lens L2 to the sample in a special rotating cuvette. The fluorescence of the sample is focused by parabolic mirrors M5 and M6 onto a nonlinear crystal, where it interacts with the gate pulse and generates radiation at the sum frequency. Filter F3 is necessary to block the light from the pump pulse. The average power at the excitation wavelength was about 2.5 mW. Beam size focused on the sample - 0.2-0.3 mm.

Photochemical changes of the samples during the measurements were monitored by measuring absorption and luminescence spectra before and after the kinetics measurements.

ExciPro spectrometer optical scheme is shown in Fig. 4. The pump pulse passes through an optical chopper and is focused onto the sample cuvette. The probe pulse (800 nm) is reflected from M1, passes through apertures A1 and A2, and is then directed by mirror M2 to a retroreflector (R) installed on the delay line. After the M3-M5 mirrors, it is focused onto a white light generator (WLG) to generate a continuum in the range from 440 nm to 1700 nm. The continuum is reflected from the parabolic mirror M6, passes through the diaphragm A3 and the filter F2, which does not transmit 800 nm light, and enters the beam splitter (BS).

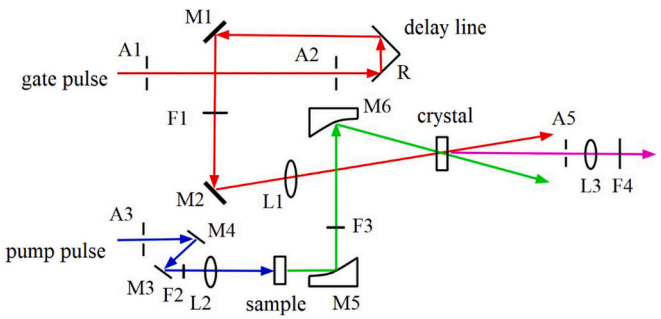

Fig. 3. Optical scheme of FOG100-DA.

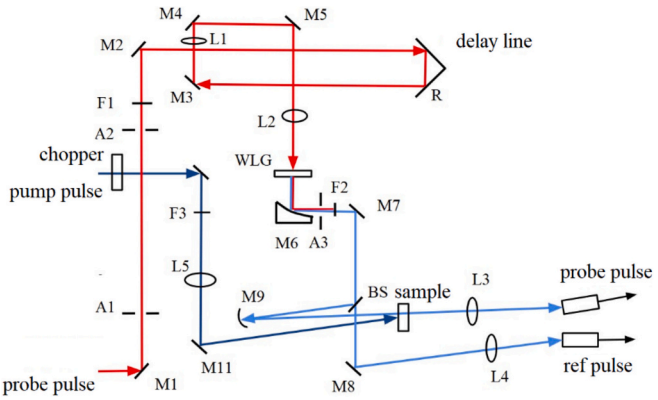

Fig. 4. Scheme of ExciPro-XL.

At the BS the beam is divided into a probe beam and a reference beam. Concave mirror M9 directs the probe beam to the sample and L3, and M8 directs the reference beam to L4. The average power at the excitation wavelength was about 0.7 mW. Beam size focused on the sample - 0.3-0.4 mm.

2.4. Computational methods

Time-dependent density-functional theory (TD-DFT) with five functionals (B3PW91, PBE0, X3LYP, B3LYP and BHandHLYP) in combination with the widely used Pople's split-valence basis sets 6-311G(d) or equivalently 6-311G* were involved to optimize the pterin structure in ground and to calculate wavelengths of vertical electron excitations (VEE) with corresponding oscillator strengths. Optimizations and VEE calculations were performed using the Gaussian16 [37].

The absorption spectrum were generated by applying the vibrationally averaged statistical QM/MD (SQMMD) technique [38,39] extended to eSQMMD due to QM motion driven by acceleration forces through gradient calculations [34,40]. In this approach instantaneous fluctuating conformers are chosen along a quantum-classical Molecular Dynamics (QCMD) trajectory for conventional TD-DFT VEE calculations. The numerous excited states of the static structural snapshots is converted into an optical spectrum from the same number of propagation time points due to the ergodic hypothesis [38]. The structural parameters and driving forces of unexcited H_4Bip were obtained using BHandHLYP&6-31G* on the $t = 5$ ps QCMD trajectory with the time step $\tau = 0.5$ fs that provided 2000 snapshots for B3LYP&6-311G* VEE calculations. 2000 molecular configurations from 10,000 steps were taken for statistical averaging of the first four excitation bands and were integrated through averaging over oscillator strengths Δf for each $\Delta\lambda$ chosen on the total spectrum from the shortest to longest wavelengths.

MRSF calculates electronic excitations due to superpositions of spin-flip orbital transitions originating from a triplet reference state [32–34,41]. The method is most often and successfully combined with the BHandHLYP&6-311G* for CoIn searching between molecular electronic states [32,34,41,42] and NAMD propagation pathways of the excited energy dissipation and probabilities of electronic transitions [33,34,42] for small organic molecules [34,36,42,43] because of 50 % Hartree-Fock contribution to the Becke's half-and-half exchange + LYP functional [44,45]. TD-BHandHLYP is the same family as the widely used popular TD-B3LYP [46] which usually returns reasonably good accuracy for organic molecules excitations, but BHandHLYP is the most appropriate of ultrafast photodynamics.

A comparison of different functionals is shown in Fig. S1. For all approximations, the lowest excited state is of ππ* nature. The best agreement with the experimental absorption spectrum is observed for the B3LYP, X3LYP, B3PW91 functionals. In comparison, the accuracy of UV–vis spectrum for pterin is performed with the following order:

B3LYP > PBE0 ≈ X3LYP > CAM-B3LYP [1]. The original experimental optical data verify the results obtained at TD-B3LYP and TD-BHandHLYP for optimizations and VEE calculations.

In this work, CoIns were determined using MRSF with BHandHLYP&6-311G* in two ways as direct crossings between the lowest excited and ground states vs two-stage transitions from the second excitation to the ground state through intermediate exited states. The 6-311G* basis set [47] is usually the minimum requirement to accurately describe the experimental photodynamic evolution. 6-31G* provides insignificant difference with the lager basis set especially for non-heavy elements but it saves computational resources to simulate 1000 steps NAMD propagation for five MRSF electronic states of the large molecule. NAMD provides $t = 400$ fs photodynamical dissipations through crossing points of electronically excited PESes to the ground state by means of MRSF calculations accompanied by the stochastic trajectory surface hopping (TSH) methods [48] and driving accelerations through gradient calculations [34,36]. The calculations for similar systems (adenine and guanine) were performed recently [49] and justify the application of MRSF/BHandHLYP methodology to H_4Bip. The main limitation of the MRSF method is computational cost: the method often involves calculations in high-dimensional spaces, which can lead to a significant increase in computational resources: memory and processing time.

3. Results and discussion

3.1. Time-resolved spectroscopy

Figure 5 shows absorption and luminescence spectra of H_4Bip at neutral pH (pH 7.5) and their evolution over time. The spectra of H_4Bip autoxidation/photo-oxidation have been studied by us in previous publications in sufficient details [20,50]. H_4Bip has a longwave maximum located at 298 nm, whereas the maximum of H_2Bip is located at 325 nm, the maximum of Bip is at 346 nm. One can determine the concentrations of pterins using solely absorption spectra [50]. Regarding Fig. 5, one can see that H_4Bip is oxidized into H_2Bip, which results in the absorption maximum at 325; Bip is also formed to a lesser extent. As can be seen, the fresh solution does not exhibit noticeable luminescence. However, over time, the sample begins to exhibit luminescence related to oxidized forms of pterins, as evidenced by the corresponding absorption spectra similar to an oxidized form observed earlier with literature data [20].

Figure 6 shows the fluorescence decay curve at 345 nm. Table 1 shows the results of the decay curves fitting using a 3-exponential model and a Gaussian apparatus function with a half-maximum width of 250 fs.

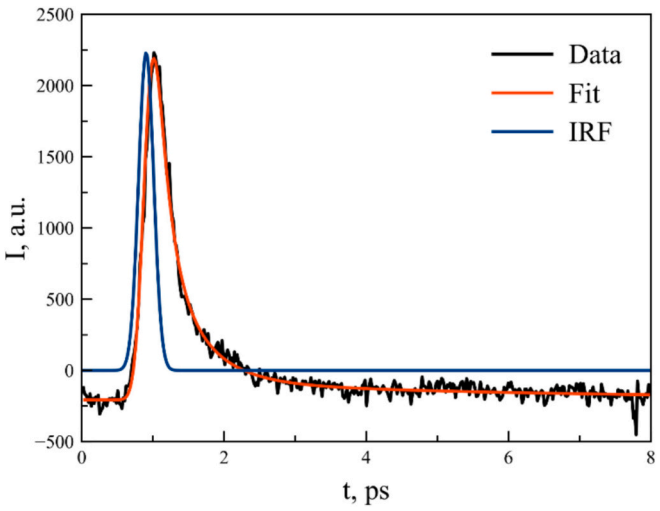

Fig. 6. H_4Bip (3 mM) fluorescence decay curve in phosphate buffer (pH 7.5) and a fit with 3-exponential functions (emission wavelength is at 345 nm).

Table 1
Pre-exponential coefficients and luminescence decay times of H_4Bip (3 mM) in phosphate buffer (pH 7.5).

Instrument response function (IRF) with a width of 250 fs			
a1	0.68	t1, ps	0.17 ± 0.07
a2	0.29	t2, ps	0.5 ± 0.2
a3	0.03	t3, ps	5 ± 2

Fig. S3 (see ESI) shows the absorption spectra before and after the kinetic measurement.

Thus, three extremely short luminescence lifetimes on femtosecond time scales were obtained for samples prepared in a nitrogen atmosphere box. Moreover, the long-lived component t3 cannot be unambiguously classified. Such small lifetimes are consistent with the extremely low fluorescence of H_4Bip [51] (it is practically not observed under continuous excitation in the steady-state spectrum). For comparison, a similar rapid internal conversion is observed for DNA nucleobases [52].

For H_4Bip samples prepared in phosphate buffer using a nitrogen atmosphere box, the transient absorption spectra were measured by the pump-probe method when excited by a pulse at a wavelength of 270 nm. Fig. 7 shows the transient absorption spectra for different delay times.

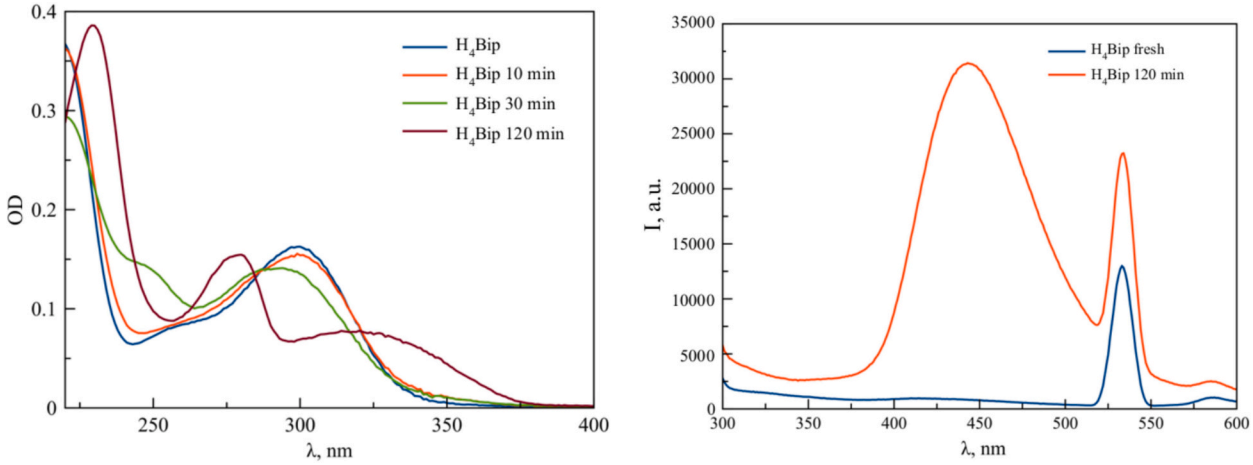

Fig. 5. Evolution of absorption (on the left) and luminescence (on the right) spectra of 41 μM H_4Bip in air-equilibrated aqueous solution (50 mM phosphate buffer, pH 7.5) over time. Signal at 535 nm is attributed to Raman scattering of the solvent.

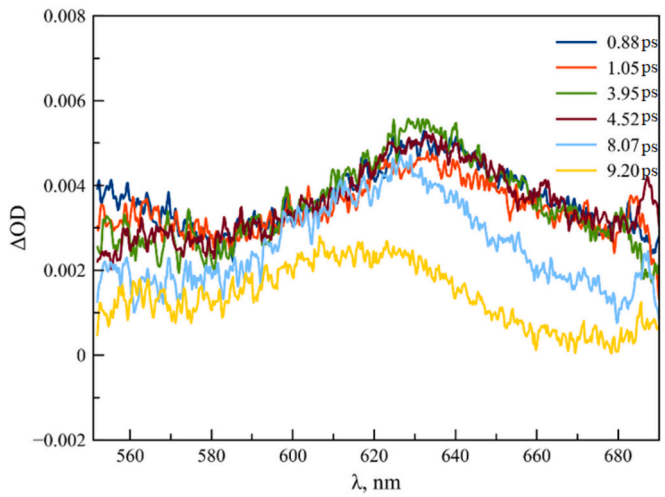

Fig. 7. Transient absorption spectra of H_4Bip (3 mM, pH 7.5) in a nitrogen atmosphere at different delay times, $\lambda_{exc} = 270$ nm.

The selected values are characterized by ΔOD > 0 with a maximum in the region of 630 nm. With an increase in the delay time, a shift of 10 nm to the shortwave region is noticeable.

Figure S4 of the ESI shows the steady-state absorption spectra recorded before and after the measurements on the ExciPro setup. During the measurements, the absorption increases by about 5 % at the pump wavelength ($\lambda_{exc} = 270$ nm), indicating a photochemical process.

Figure 8 shows a transient absorption trace of H_4Bip at 580 nm. In contrast to the fluorescent decay, the main transient absorption component decays on picosecond time scale with a lifetime of 10 ps. It may be associated with the population of nπ* and ICT states. For example, these states were supposed to be involved in the deactivation pathways of nucleobases [53]. The formation of these states with a characteristic rise time of 0.7 ps (close to the fluorescence lifetime t_2 in Table 1) can be seen in the transient absorption trace at 640 nm (Fig. S5).

Rapid deactivation of the excitation of H_4Bip on subpicosecond and picosecond time scales is similar to that observed in nucleobases [54,55]. Different decay lifetimes obtained from the pump-probe and fluorescence up-conversion experiments reflect different deactivation mechanisms of the excited states of H_4Bip. While the fast process with the characteristic lifetimes of 0.17 and 0.5 ps can be referred as internal conversion from the lowest ππ* state, the slow process with the characteristic lifetime of 10 ps is probably associated with relatively dark (non-fluorescent) state. This state can be of nπ* or intramolecular charge transfer (ICT) nature. Two distinct internal conversion channels with nπ* or ICT states have been discussed for nucleobases [53,56].

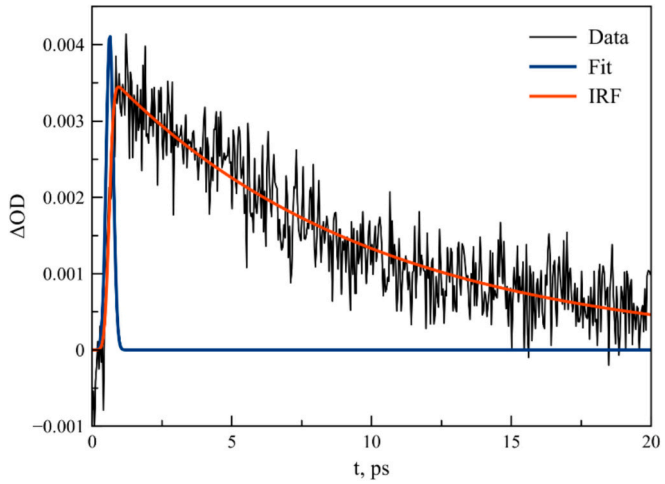

Fig. 8. Transient absorption decay of H_4Bip (3 mM, pH 7.5) at 580 nm ($\lambda_{exc} = 270$ nm). Single-exponential fit yields a characteristic lifetime of 10 ± 1 ps.

3.2. *Quantum chemical calculations*

First, we chose the optimal combination of functional and basis set, comparing the results of calculations for H_4Bip with the experimental data and literature data for 7-deazaguanosine. Table 2 shows five electronic states of 7-deazaguanosine and H_4Bip molecules calculated at the same level of theory: TDDFT/PBE0 with the same Pople basis set. Moreover, a comparison of B3LYP, PBE0 and BHandHLYP performance predicting the absorption spectrum of H_4Bip can be found on Fig. S1.

7-Deazaguanine is similar to H_4Bip possessing a pyrimidine ring accompanied by the amino group and carbonyl, which also largely determines the similarity of guanine and H_4Bip photophysics: it is the six-membered azaheterocycle accompanied by the NH_2 group and carbonyl. The pyrimidine largely determines the photophysics of both H_4Bip and guanine. Previously, we have compared the photophysics of H_4pterin and guanine using quantum chemistry methods: in particular, we showed that the excited states and CoIn have similar nature and geometry [16]. Thus, the results obtained for H_4Bip and 7-deazaguanine are in good agreement (Table 2).

Next, the absorption spectrum was calculated using the B3LYP/6-311G* method and quantum dynamics (Fig. 9). Instantaneous 2000 vibrationally fluctuating structural snapshots of pterin were extracted after each 10 steps on the 5 ns quantum chemistry MD trajectory. All spectral intensities were normalized to unity. Absorption spectra were generated on all selected vibrational conformers with a resolution of 2 nm in terms of wavelengths.

According to MD simulations the major peak of H_4Bip absorption spectrum is located at 301 nm close to the maximum observed at 298 nm in a neutral aqueous solution [20]. Another energy maximum is located at 257 nm, which is also close to the experiment peak at 254 nm. It is worth noting the presence of *nπ** and πσ* (or so-called intramolecular charge transfer ICT state) states with low oscillator strengths in this spectral range. In the case of 7-deazaguanine and guanosine monophosphate, the ICT state was considered as a second channel of internal conversion.

CoIn searching was initiated from Franck–Condon (FC) excited states of the ground state optimized structure. The CoIn searching occurred both from the lowest excited state and from the higher excitation in two stages, to the lowest excited state and then to the ground state (Fig. 10). It should be noted that the direct transition from the lowest Frank-Condon state has a higher energy barrier than the two-step transition from the next Frank-Condon excited state, which turns out to be energetically more favorable and most probable for the transition to the ground state.

Electron densities ρ of various states are obtained within the framework of MRSF calculations, along with Dyson molecular orbitals (DMO) based on the extended Koopmans' theorem (DMO-EKT) [57–59] defining the EDD shapes and types of single-configurational transitions. These transitions are based on the promotion of electrons from higher doubly occupied (norm = 1) DMO $|HDDO\rangle_{GS}$ of ground state, corresponding to the lowest half-occupied (norm ≈ 0.5) DMO $|LSDO\rangle_{Si}$ of the *i*-th excited state, to the highest singly occupied (norm ≈ 0.5) DMO $|HSDO\rangle_{Si}$. This approach works with multiconfigurational methods in contrast with canonical MOs, which are inapplicable to the spin-flip methodology. In this work, electron densities were reconstructed from DMOs eigenvectors calculated in GAMESS. DMOs, analogously to Natural Orbitals (NO), allow one-electron excitations to be presented in a chemically oriented, single-configurational HOMO-LUMO type transitions, while also providing orbital and transition energies.

NAMD propagates photodynamic trajectories of several excited states with their PESs stochastically crossing through CoIn points using

Table 2
Main electron transitions of 7-deazaguanosine and H_4Bip molecules.

	7-deazaguanosine [56]			H_4Bip: PBE0/6–311 + G(d,p), iefpcm			H_4Bip: PBE0/6–311 + G(d,p), gas phase		
states	transitions	%	*E*(eV)	transitions	%	*E*(eV)	transitions	%	*E*(eV)
$S_1(\pi\pi^*)$	H-0 → L + 0	97	4.66 (0.1448)	H-0 → L + 0	89	4.84(0.2631)	H-0 → L + 0	97	4.82(0.0296)
	H-0 → L + 1	3		H-0 → L + 1	8				
$S_2(\pi\pi^*)$	H-0 → L + 0	3	4.98 (0.3044)	H-0 → L + 0	8	5.15(0.5923)	H-0 → L + 1	95	4.99(0.1364)
	H-0 → L + 1	93		H-0 → L + 1	90				
$S_3(\pi\sigma^*)$	H-0 → L + 2	95	5.2 (0.0026)	H-0 → L + 2	96	5.45(0.0008)	H-0 → L + 3	97	5.38(0.0070)
							H-0 → L + 2	91	5.31(0.2509)
$S(n\pi^*)$	H-3 → L + 0	74	5.6 (0.0019)	H-1 → L + 0	78	5.61(0.0003)	H-1 → L + 1	34	5.32(0.0068)
	H-0 → L + 3	12		H-2 → L + 0	18		H-2 → L + 2	51	

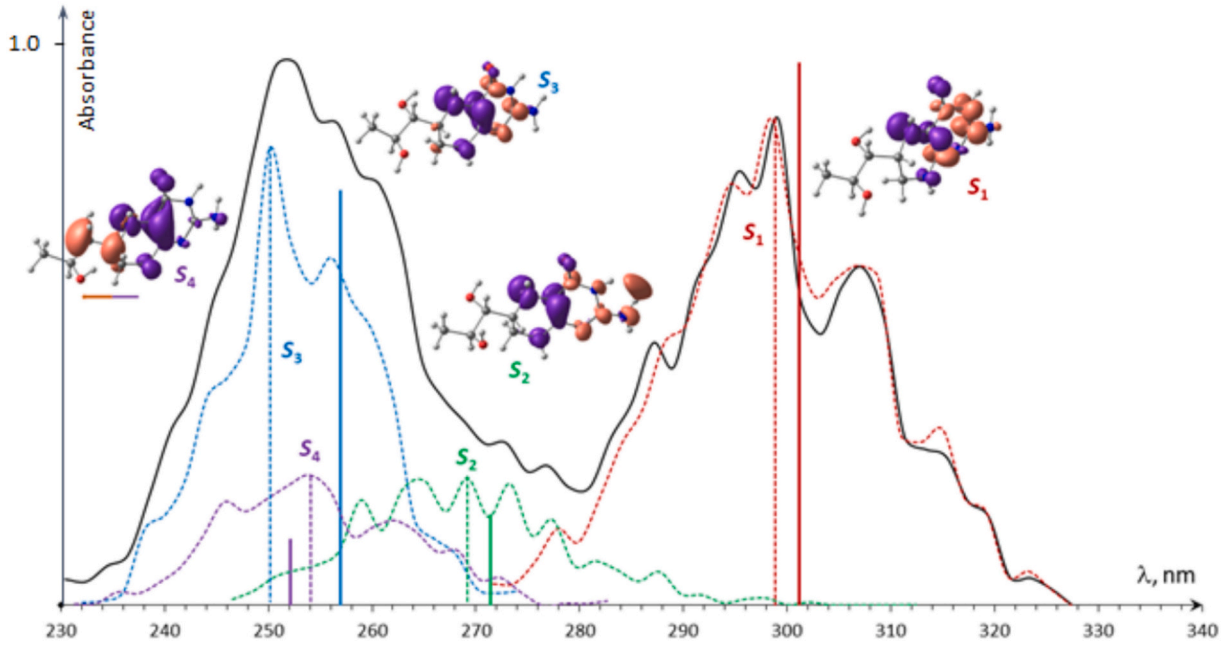

Fig. 9. The statistical absorption spectra of H_4Bip (solid curve) with bands decomposition (dashed lines) and VEE of optimized structure (verticals) of S_{1-4} (red, green, blue and violet, respectively). Electron density redistribution $\Delta\rho_{0\to i=1-4} \approx |\mathrm{LUMO}+i-1\rangle^2 - |\mathrm{HOMO}\rangle^2$ from violet to orange areas on structures at spectral maxima (dashed verticals). Intensities are normalized and scaled to the maximal oscillator strength. (For interpretation of the references to colour in this figure legend, the reader is referred to the web version of this article.)

the random function of the trajectory surface hopping (TSH) method. This approach provides statistically averaged lifetimes of excitations but requires running hundreds of NAMD trajectories from various initial vibrational conditions, which is extremely time-consuming and unstable for even small molecules and outside the current scope of interest. However, the types of CoIn transitions are defined solely by the nature of crossing electronic states, which can be investigated using one or several trajectories with the same initial conditions. NAMD simulation was initiated from Frank-Condon $S_4(\pi \to \pi^*)$ of the optimized unexcited system (Fig. 11) of the H_4pterin chromophore, optimized in the ground state, for the dissipative evolution of the excited molecule until relaxation to a vibrational mode in the ground state. This was done to compare molecular space structural deformations depending on the level of initial excitation in the manner of CoIn searching.

NAMD trajectories of states starting from the structure optimized in the ground and corresponding Frank-Condon excited states were also calculated (Fig. 11). Usage of the BHandHLYP functional [44] gives the best agreement with the experiment: starting from the 4th excited state, the system quickly (within 50 fs) passes to the lower excited state, and after 200 fs a clear conical intersection with the ground state is observed. A sequential model of a probabilistic NAMD trajectory demonstrated swift transitions from S_4 through S_3 to S_1 along $t(S_4 \to S_2 \to S_1) = 55.5$ fs and final excitation decay at $t(S_1 \to S_0) = 214.5$ fs.

7-Deazaguanine is similar to H_4Bip possessing a pyrimidine ring accompanied by the amino group and carbonyl, which also largely determines the similarity of guanine and H_4Bip photophysics: the pyrimidine largely determines the photophysics of both H_4Bip and guanine [16]. In comparison with fs-fluorescence and fs-transient absorption experiments, theoretical analysis revealed some important points. First, TD-DFT calculations determined the presence of $n\pi^*$ and ICT states, similar to those obtained in 7-deazaguanosine. These states can be responsible for the second slow relaxation channel observed in the transient absorption decay of H_4Bip. Second, non-adiabatic dynamics trajectory revealed a fast relaxation channel from S_1 $\pi\pi^*$ state via internal conversion to the ground state. The characteristic time of this relaxation appeared to be close to the fluorescence life time. At the moment, we have no proof of the slow relaxation path by the NAMD simulations. This fact can be explained with further investigation of numerous (300 and more simulations) stochastic trajectories of excitation evolutions to define scenario of much longer dissipation life time.

4. Conclusion

Our experimental findings using fs-fluorescence up-conversion and fs-transient absorption spectroscopy show that the excited states of H_4Bip deactivate both on subpicosecond and picosecond time scales.

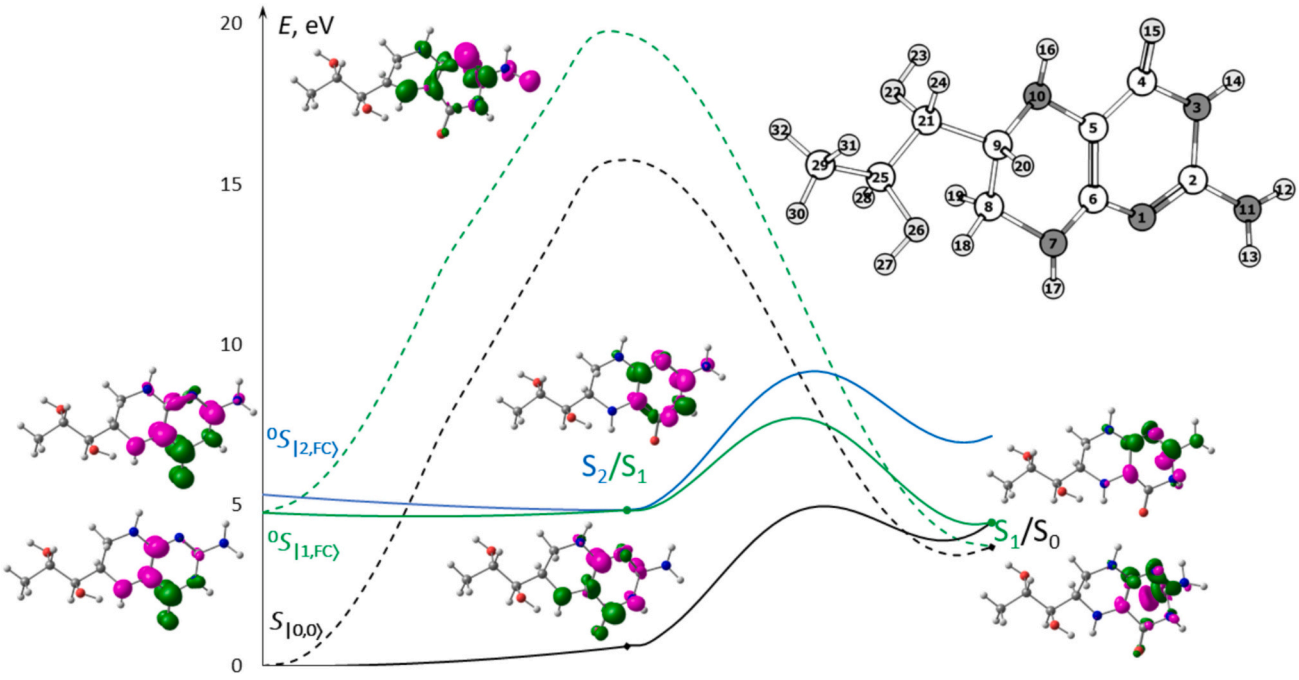

Fig. 10. CoIn $S_2 \rightarrow S_1 \rightarrow S_0$ vs $S_1 \rightarrow S_0$ (green and black dashed lines, respectively) reaction pathways from FC and $S_{|0,0\rangle}$ states through CoIn. $S_0 \rightarrow S_j$ excitation $EDD_{ex} = \rho(S_{j=1,2})\text{-}\rho(S_0)$ and $S_j \rightarrow S_0$ dissipation $EDD_{dis} = \rho(S_i)\text{-}\rho(S_{i+1})$ EDD increase from green to pink areas. (For interpretation of the references to colour in this figure legend, the reader is referred to the web version of this article.)

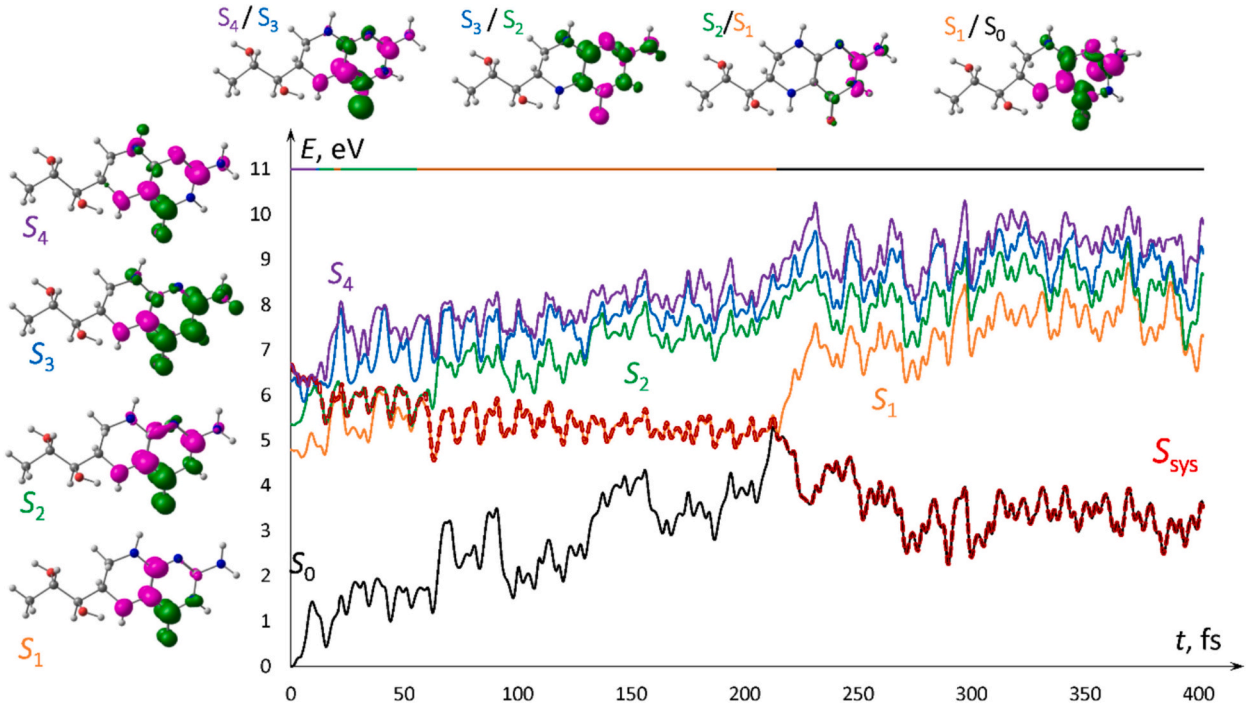

Fig. 11. NAMD PES (in respect to E_{min}) trajectories starting from ground state optimized H_4Bip vertically excited in the S_4 (violet), S_3 (blue), S_2 (green), the lowest excited state S_1 (yellow) and the ground state S_0 (black). S_{sys} (dashed red) is the main deactivation channel. EDD for the initial optimized structure and at crossing points. (For interpretation of the references to colour in this figure legend, the reader is referred to the web version of this article.)

Major fluorescent components decay via internal conversion from the S_1 state within hundreds of femtoseconds, whereas fs-transient absorption reveals a second relaxation mechanism with a characteristic life time of several picoseconds. The latter may be associated with population of nπ* or ICT states. The presence of these states is supported by the corresponding TD-DFT calculations. Nonadiabatic molecular dynamic using the MRSF approach reveal a fast (within ca. 200 fs) deactivation of S_4-S_1 states of H_4Bip via a conical intersection, which agrees well with the experimentally observed life times of the fluorescence decay. Multiple deactivation pathways on subpicosecond and picosecond time scales observed for H_4Bip resemble the behavior of isolated DNA nucleobases.

These findings lead to several conclusions. First, H_4Bip as a

coenzyme is not oxidized on a subpicosecond-timescale due to the ultrafast internal conversion. However, the photo-oxidation of H_4Bip probably occurs on a larger time-scale of nanoseconds (the photo-oxidation of H_4Bip has been studied in sufficient details previously [20,50]), which can lead, for example, to tyrosinase photo-switch [15]. The 3–5-fold excess of H_4Bip in vivo inhibits tyrosinase, which is a well-known effect [25]. Thus, the photoinactivation of H_4Bip stimulates tyrosinase [15]. The mechanism of tyrosinase inhibition by H_4Bip is unknown, but the detailed information on the structure of tyrosinase active site and its inhibition can be found in recent publications [60]. Apparently, H_4Bip could interact with Arg209 and His208 residues in the active site of tyrosinase.

Second, H_4cyanopterin and H_4Bip as photoreceptor molecules can participate in photoreception of UVB, however, its mechanism is largely unknown. We can suggest a photoinduced electron transfer (PET) and/or a photosensitized oxidation of H_4Bip [50]. It is possible that PET may account for the observed activity at 10–30 fs [61] (H_4Bip is a strong antioxidant and can easily loose electrons [62]; however, further investigation would be needed, including time-resolved spectroscopy and ab initio molecular dynamics). The rest of possible mechanisms are slow: for example, phototransformation of flavin in photoreceptor proteins (LOV-based proteins, etc.) occurs on a nano-second timescale with a lifetime of ca. 5 ns in the case of FMN [63] or 15 ps in the case of flavin [64] (flavins are a related group of compounds also known as benzopteridines).

CRediT authorship contribution statement

Varvara G. Kubenko: Writing – original draft, Visualization, Investigation, Formal analysis. **Vladimir A. Pomogaev:** Writing – original draft, Visualization, Investigation, Formal analysis. **Andrey A. Buglak:** Writing – original draft, Funding acquisition, Conceptualization. **Alexei I. Kononov:** Writing – review & editing, Supervision.

Declaration of competing interest

The authors declare that they have no known competing financial interests or personal relationships that could have appeared to influence the work reported in this paper.

Acknowledgements

This work was supported by the Russian Science Foundation grant 20-73-10029 (https://rscf.ru/en/project/20-73-10029/#!). Spectral measurements were performed using equipment from the Centre for Optical and Laser Materials Research (https://researchpark.spbu.ru/en/laser-eng).

Appendix A. Supplementary data

Supplementary data to this article can be found online at https://doi.org/10.1016/j.jphotobiol.2025.113134.

Data availability

Data will be made available on request.

References

[1] A.A. Buglak, M.A. Kapitonova, Y.L. Vechtomova, T.A. Telegina, Insights into molecular structure of Pterins suitable for biomedical applications, Int. J. Mol. Sci. 23 (2022) 15222, https://doi.org/10.3390/ijms232315222.
[2] T. Eichwald, L. de B. da Silva, A.C. Staats Pires, L. Niero, E. Schnorrenberger, C. C. Filho, G. Espíndola, W.L. Huang, G.J. Guillemin, J.E. Abdenur, A. Latini, Tetrahydrobiopterin: beyond its traditional role as a cofactor, Antioxidants 12 (2023) 1–27, https://doi.org/10.3390/antiox12051037.
[3] E. Alhajji, A. Boulghobra, M. Bonose, F. Berthias, F. Moussa, P. Maître, Multianalytical approach for deciphering the specific MS/MS transition and overcoming the challenge of the separation of a transient intermediate, Quinonoid dihydrobiopterin, Anal. Chem. 94 (2022) 12578–12585, https://doi.org/10.1021/acs.analchem.2c00924.
[4] S. Samanta, P. Mondal, A comprehensive computational study on the thermodynamics and kinetics of tetrahydrobiopterin regeneration process, ChemPhysChem 2024 (2024) 19–22, https://doi.org/10.1002/cphc.202400401.
[5] T. Malcomson, M.J. Paterson, Theoretical determination of two-photon absorption in biologically relevant pterin derivatives, Photochem. Photobiol. Sci. 19 (2020) 1538–1547, https://doi.org/10.1039/d0pp00255k.
[6] T. Malcomson, Determination of two-photon absorption in nucleobase analogues: a QR-DFT perspective, Photochem. Photobiol. Sci. 21 (2022) 529–543, https://doi.org/10.1007/s43630-022-00182-7.
[7] U. Gallaga-González, E. Morales-Avila, E. Torres-García, J.A. Estrada, L.E. Díaz-Sánchez, G. Izquierdo, L. Aranda-Lara, K. Isaac-Olivé, Photoactivation of chemotherapeutic agents with Cerenkov radiation for chemo-photodynamic therapy, ACS Omega 7 (2022) 23591–23604, https://doi.org/10.1021/acsomega.2c02153.
[8] J.V. Correia, B. Wilke, C. Schulzke, Synthesis, characterization and chlorination of 4-(Pentyloxy)-7-(prop-2-yn-1-yloxy)pteridin-2-amine, Molbank 2023 (2023), https://doi.org/10.3390/M1692.
[9] A.H. Thomas, C. Lorente, A.L. Capparelli, C.G. Martínez, A.M. Braun, E. Oliveros, Singlet oxygen (1Δg) production by pterin derivatives in aqueous solutions, Photochem. Photobiol. Sci. 2 (2003) 245–250, https://doi.org/10.1039/B209993D.
[10] A.A. Buglak, T.A. Telegina, E.A. Vorotelyak, A.I. Kononov, Theoretical study of photoreactions between oxidized pterins and molecular oxygen, J. Photochem. Photobiol. A Chem. 372 (2019) 254–259, https://doi.org/10.1016/j.jphotochem.2018.12.002.
[11] M.P. Serrano, C. Lorente, C.D. Borsarelli, A.H. Thomas, Unraveling the degradation mechanism of purine nucleotides photosensitized by Pterins: the role of charge-transfer steps, ChemPhysChem 16 (2015) 2244–2252, https://doi.org/10.1002/cphc.201500219.
[12] M.L. Dantola, L.O. Reid, C. Castaño, C. Lorente, E. Oliveros, A.H. Thomas, Photosensitization of peptides and proteins by pterin derivatives, Pteridines 28 (2017) 105–114, https://doi.org/10.1515/pterid-2017-0013.
[13] C. Lorente, M.P. Serrano, M. Vignoni, M.L. Dántola, A.H. Thomas, A model to understand type I oxidations of biomolecules photosensitized by pterins, J. Photochem. Photobiol. 7 (2021) 100045, https://doi.org/10.1016/j.jpap.2021.100045.
[14] J.M. Wood, K.U. Schallreuter-Wood, N.J. Lindsey, S. Callaghan, M.L. Gardner, A specific tetrahydrobiopterin binding domain on tyrosinase controls melanogenesis, Biochem. Biophys. Res. Commun. 206 (1995) 480–485, https://doi.org/10.1006/bbrc.1995.1068.
[15] K.U. Schallreuter, J.M. Wood, C. Körner, K.M. Harle, V. Schulz-Douglas, E. R. Werner, 6-tetrahydrobiopterin functions as a UVB-light switch for de novo melanogenesis, Biochim. Biophys. Acta 1382 (1998) 339–344, https://doi.org/10.1016/s0167-4838(97)00178-7.
[16] A.A. Buglak, T.A. Telegina, A theoretical study of 5,6,7,8-tetrahydro-6-hydroxymethylpterin: insight into intrinsic photoreceptor properties of 6-substituted tetrahydropterins, Photochem. Photobiol. Sci. 18 (2019) 516–523, https://doi.org/10.1039/C8PP00322J.
[17] Y.-J. Moon, S.-J. Kim, Y.M. Park, Y.-H. Chung, Sensing UV/blue: pterin as a UV-A absorbing chromophore of cryptochrome, Plant Signal. Behav. 5 (2010) 1127–1130, https://doi.org/10.4161/psb.5.9.12567.
[18] Y.-J. Moon, S. Il Kim, Y.-H. Chung, Sensing and responding to UV-A in cyanobacteria, Int. J. Mol. Sci. 13 (2012) 16303–16332, https://doi.org/10.3390/ijms131216303.
[19] J. Takeda, R. Nakata, H. Ueno, A. Murakami, M. Iseki, M. Watanabe, Possible involvement of a tetrahydrobiopterin in photoreception for UV-B-induced anthocyanin synthesis in carrot, Photochem. Photobiol. 90 (2014) 1043–1049, https://doi.org/10.1111/php.12302.
[20] T.A. Telegina, T.A. Lyudnikova, A.A. Buglak, Y.L. Vechtomova, M.V. Biryukov, V. V. Demin, M.S. Kritsky, Transformation of 6-tetrahydrobiopterin in aqueous solutions under UV-irradiation, J. Photochem. Photobiol. A Chem. 354 (2018) 155–162, https://doi.org/10.1016/j.jphotochem.2017.07.029.
[21] A.A. Buglak, T.A. Telegina, Y.L. Vechtomova, M.S. Kritsky, Autoxidation and photooxidation of tetrahydrobiopterin: a theoretical study, Free Radic. Res. 55 (2021) 499–509, https://doi.org/10.1080/10715762.2020.1860213.
[22] M. Vignoni, F.M. Cabrerizo, C. Lorente, A.H. Thomas, New results on the photochemistry of Biopterin and Neopterin in aqueous solution, Photochem. Photobiol. 85 (2009) 365–373, https://doi.org/10.1111/j.1751-1097.2008.00450.x.
[23] M.L. Dántola, M. Vignoni, A.L. Capparelli, C. Lorente, A.H. Thomas, Stability of 7,8-Dihydropterins in air-equilibrated aqueous solutions, Helv. Chim. Acta 91 (2008) 411–425, https://doi.org/10.1002/hlca.200890046.
[24] E. Oliveros, M.L. Dántola, M. Vignoni, A.H. Thomas, C. Lorente, Production and quenching of reactive oxygen species by pterin derivatives, an intriguing class of biomolecules, Pure Appl. Chem. 83 (2010) 801–811, https://doi.org/10.1351/PAC-CON-10-08-22.
[25] T.A. Telegina, Y.L. Vechtomova, V.A. Borzova, A.A. Buglak, Tetrahydrobiopterin as a trigger for vitiligo: Phototransformation during UV irradiation, Int. J. Mol. Sci. 24 (2023) 13586, https://doi.org/10.3390/ijms241713586.
[26] H.W. Lee, C.H. Oh, A. Geyer, W. Pfleiderer, Y.S. Park, Characterization of a novel unconjugated pteridine glycoside, cyanopterin, in Synechocystis sp. PCC 6803, Biochim. Biophys. Acta 1410 (1999) 61–70, https://doi.org/10.1016/s0005-2728(98)00175-3.

[27] M.Z. Zgierski, T. Fujiwara, E.C. Lim, Conical intersections and ultrafast intramolecular excited-state dynamics in nucleic acid bases and electron donor–acceptor molecules, Chem. Phys. Lett. 463 (2008) 289–299, https://doi.org/10.1016/j.cplett.2008.06.024.
[28] A. Munoz-Losa, M. Martín, I. Galván, M. Aguilar Yuste, Location of conical intersections in solution using a sequential quantum mechanics/molecular dynamics method, Chem. Phys. Lett. 443 (2007) 76–81, https://doi.org/10.1016/j.cplett.2007.06.037.
[29] Y. Wang, D.A. Mazziotti, Quantum simulation of conical intersections, Phys. Chem. Chem. Phys. 26 (2024) 11491–11497, https://doi.org/10.1039/D4CP00391H.
[30] A.V. Bochenkova, Multiconfigurational Methods Including XMCQDPT2 Theory for Excited States of Light-Sensitive Biosystems, in: Compr. Comput. Chem., Elsevier, 2024, pp. 141–157, https://doi.org/10.1016/B978-0-12-821978-2.00133-1.
[31] J. Segarra-Martí, M. Garavelli, F. Aquilante, Multiconfigurational second-order perturbation theory with frozen natural orbitals extended to the treatment of photochemical problems, J. Chem. Theory Comput. 11 (2015) 3772–3784, https://doi.org/10.1021/acs.jctc.5b00479.
[32] S. Lee, E.E. Kim, H. Nakata, S. Lee, C.H. Choi, Efficient implementations of analytic energy gradient for mixed-reference spin-flip time-dependent density functional theory (MRSF-TDDFT), J. Chem. Phys. 150 (2019) 184111, https://doi.org/10.1063/1.5086895.
[33] W. Park, S. Lee, M. Huix-Rotllant, M. Filatov, C.H. Choi, Impact of the dynamic electron correlation on the unusually long excited-state lifetime of thymine, J. Phys. Chem. Lett. 12 (2021) 4339–4346, https://doi.org/10.1021/acs.jpclett.1c00712.
[34] M. Huix-Rotllant, K. Schwinn, V. Pomogaev, M. Farmani, N. Ferré, S. Lee, C. H. Choi, Photochemistry of thymine in solution and DNA revealed by an electrostatic embedding QM/MM combined with mixed-reference spin-Flip TDDFT, J. Chem. Theory Comput. 19 (2023) 147–156, https://doi.org/10.1021/acs.jctc.2c01010.
[35] M. Huix-Rotllant, N. Ferré, Analytic energy, gradient, and hessian of electrostatic embedding QM/MM based on electrostatic potential-fitted atomic charges scaling linearly with the MM subsystem size, J. Chem. Theory Comput. 17 (2021) 538–548, https://doi.org/10.1021/acs.jctc.0c01075.
[36] M. Alías-Rodríguez, S. Bonfrate, W. Park, N. Ferré, C.H. Choi, M. Huix-Rotllant, Solvent effects and pH dependence of the X-ray absorption spectra of proline from electrostatic embedding quantum mechanics/molecular mechanics and mixed-reference spin-Flip time-dependent density-functional theory, J. Phys. Chem. A 127 (2023) 10382–10392, https://doi.org/10.1021/acs.jpca.3c05070.
[37] D.J. Frisch, M.J. Trucks, G.W. Schlegel, H.B. Scuseria, G.E. Robb, M.A. Cheeseman, J.R. Scalmani, G. Barone, V. Petersson, G.A. Nakatsuji, H. Li, X. Caricato, M. Marenich, A.V. Bloino, J. Janesko, B.G. Gomperts, R. Mennucci, B. Hratch, M. J. Frisch, G.W. Trucks, H.B. Schlegel, G.E. Scuseria, M.A. Robb, J.R. Cheeseman, G. Scalmani, V. Barone, G.A. Petersson, H. Nakatsuji, X. Li, M. Caricato, A. V. Marenich, J. Bloino, B.G. Janesko, R. Gomperts, B. Mennucci, H.P. Hratchian, J. V. Ortiz, A.F. Izmaylov, J.L. Sonnenberg, D. Williams-Young, F. Ding, F. Lipparini, F. Egidi, J. Goings, B. Peng, A. Petrone, T. Henderson, D. Ranasinghe, V. G. Zakrzewski, J. Gao, N. Rega, G. Zheng, W. Liang, M. Hada, M. Ehara, K. Toyota, R. Fukuda, J. Hasegawa, M. Ishida, T. Nakajima, Y. Honda, O. Kitao, H. Nakai, T. Vreven, K. Throssell, J.A. Montgomery Jr., J.E. Peralta, F. Ogliaro, M. J. Bearpark, J.J. Heyd, E.N. Brothers, K.N. Kudin, V.N. Staroverov, T.A. Keith, R. Kobayashi, J. Normand, K. Raghavachari, A.P. Rendell, J.C. Burant, S.S. Iyengar, J. Tomasi, M. Cossi, J.M. Millam, M. Klene, C. Adamo, R. Cammi, J.W. Ochterski, R.L. Martin, K. Morokuma, O. Farkas, J.B. Foresman, D.J. Fox, Gaussian16 Revision C.01, Gaussian, Inc, Wallin, 2016.
[38] V. Pomogaev, A. Pomogaeva, P. Avramov, K.J. Jalkanen, S. Kachin, Thermodynamical contours of electronic-vibrational spectra simulated using the statistical quantum–mechanical methods, Theor. Chem. Accounts 130 (2011) 609–632, https://doi.org/10.1007/s00214-011-0936-6.
[39] V.A. Pomogaev, R.R. Ramazanov, K. Ruud, V.Y. Artyukhov, Insight into the fluorescence quenching of Trp214 at HSA by the Dimetridazole ligand from simulation, J. Photochem. Photobiol. A Chem. 354 (2018) 86–100, https://doi.org/10.1016/j.jphotochem.2017.08.041.
[40] T.J. Zuehlsdorff, S.V. Shedge, S.-Y. Lu, H. Hong, V.P. Aguirre, L. Shi, C.M. Isborn, Vibronic and environmental effects in simulations of optical spectroscopy, Annu. Rev. Phys. Chem. 72 (2021) 165–188, https://doi.org/10.1146/annurev-physchem-090419-051350.
[41] W. Park, K. Komarov, S. Lee, C.H. Choi, Mixed-reference spin-Flip time-dependent density functional theory: multireference advantages with the practicality of linear response theory, J. Phys. Chem. Lett. 14 (2023) 8896–8908, https://doi.org/10.1021/acs.jpclett.3c02296.
[42] S. Sadiq, W. Park, V. Mironov, S. Lee, M. Filatov Gulak, C.H. Choi, prototropically controlled dynamics of cytosine photodecay, J. Phys. Chem. Lett. 14 (2023) 791–797, https://doi.org/10.1021/acs.jpclett.2c03340.
[43] W. Park, J. Shen, S. Lee, P. Piecuch, M. Filatov, C.H. Choi, Internal conversion between bright (11Bu+) and dark (21Ag–) states in s-trans-butadiene and s-trans-Hexatriene, J. Phys. Chem. Lett. 12 (2021) 9720–9729, https://doi.org/10.1021/acs.jpclett.1c02707.
[44] A.D. Becke, A new mixing of Hartree-Fock and local density-functional theories, J. Chem. Phys. 98 (1993) 1372–1377, https://doi.org/10.1063/1.464304.
[45] A. Nakata, Y. Imamura, T. Otsuka, H. Nakai, Time-dependent density functional theory calculations for core-excited states: assessment of standard exchange-correlation functionals and development of a novel hybrid functional, J. Chem. Phys. 124 (2006) 94105, https://doi.org/10.1063/1.2173987.
[46] C. Lee, W. Yang, R.G. Parr, Development of the Colle-Salvetti correlation-energy formula into a functional of the electron density, Phys. Rev. B Condens. Matter 37 (1988) 785–789, https://doi.org/10.1103/physrevb.37.785.
[47] R. Krishnan, J.S. Binkley, R. Seeger, J.A. Pople, Self-consistent molecular orbital methods. XX. A basis set for correlated wave functions, J. Chem. Phys. 72 (1980) 650–654, https://doi.org/10.1063/1.438955.
[48] P. Baudin, F. Mouvet, U. Rothlisberger, A multiple time step algorithm for trajectory surface hopping simulations, J. Chem. Phys. 156 (2022) 34107, https://doi.org/10.1063/5.0065728.
[49] W. Park, A. Lashkaripour, K. Komarov, S. Lee, M. Huix-Rotllant, C.H. Choi, Toward consistent predictions of Core/valence ionization potentials and valence excitation energies by MRSF-TDDFT, J. Chem. Theory Comput. 20 (2024) 5679–5694, https://doi.org/10.1021/acs.jctc.4c00640.
[50] A.A. Buglak, T.A. Telegina, T.A. Lyudnikova, Y.L. Vechtomova, M.S. Kritsky, Photooxidation of tetrahydrobiopterin under UV irradiation: possible pathways and mechanisms, Photochem. Photobiol. 90 (2014) 1017–1026, https://doi.org/10.1111/php.12285.
[51] R. Biondi, G. Ambrosio, F. De Pascali, I. Tritto, E. Capodicasa, L.J. Druhan, C. Hemann, J.L. Zweier, HPLC analysis of tetrahydrobiopterin and its pteridine derivatives using sequential electrochemical and fluorimetric detection: application to tetrahydrobiopterin autoxidation and chemical oxidation, Arch. Biochem. Biophys. 520 (2012) 7–16, https://doi.org/10.1016/j.abb.2012.01.010.
[52] C.T. Middleton, K. de La Harpe, C. Su, Y.K. Law, C.E. Crespo-Hernández, B. Kohler, DNA excited-state dynamics: from single bases to the double Helix, Annu. Rev. Phys. Chem. 60 (2009) 217–239, https://doi.org/10.1146/annurev.physchem.59.032607.093719.
[53] P.M. Hare, C.E. Crespo-Hernández, B. Kohler, Internal conversion to the electronic ground state occurs via two distinct pathways for pyrimidine bases in aqueous solution, Proc. Natl. Acad. Sci. USA 104 (2007) 435–440, https://doi.org/10.1073/pnas.0608055104.
[54] M. Barbatti, A.J.A. Aquino, J.J. Szymczak, D. Nachtigallová, P. Hobza, H. Lischka, Relaxation mechanisms of UV-photoexcited DNA and RNA nucleobases, Proc. Natl. Acad. Sci. 107 (2010) 21453–21458, https://doi.org/10.1073/pnas.1014982107.
[55] K. Kleinermanns, D. Nachtigallová, M.S. de Vries, Excited state dynamics of DNA bases, Int. Rev. Phys. Chem. 32 (2013) 308–342, https://doi.org/10.1080/0144235X.2012.760884.
[56] S.E. Krul, S.J. Hoehn, K.J. Feierabend, C.E. Crespo-Hernández, Excited state dynamics of 7-deazaguanosine and guanosine 5′-monophosphate, J. Chem. Phys. 154 (2021) 075103, https://doi.org/10.1063/5.0038123.
[57] J.V. Ortiz, Dyson-orbital concepts for description of electrons in molecules, J. Chem. Phys. 153 (2020) 70902, https://doi.org/10.1063/5.0016472.
[58] V. Pomogaev, S. Lee, S. Shaik, M. Filatov, C.H. Choi, Exploring Dyson's orbitals and their Electron binding energies for conceptualizing excited states from response methodology, J. Phys. Chem. Lett. 12 (2021) 9963–9972, https://doi.org/10.1021/acs.jpclett.1c02494.
[59] M. Filatov, S. Lee, H. Nakata, C.H. Choi, Computation of molecular Electron affinities using an ensemble density functional theory method, J. Phys. Chem. A 124 (2020) 7795–7804, https://doi.org/10.1021/acs.jpca.0c06976.
[60] B. Deri, M. Kanteev, M. Goldfeder, D. Lecina, V. Guallar, N. Adir, A. Fishman, The unravelling of the complex pattern of tyrosinase inhibition, Sci. Rep. 6 (2016) 34993, https://doi.org/10.1038/srep34993.
[61] F. Vismarra, F. Fernández-Villoria, D. Mocci, J. González-Vázquez, Y. Wu, L. Colaizzi, F. Holzmeier, J. Delgado, J. Santos, L. Bañares, L. Carlini, M. C. Castrovilli, P. Bolognesi, R. Richter, L. Avaldi, A. Palacios, M. Lucchini, M. Reduzzi, R. Borrego-Varillas, N. Martín, F. Martín, M. Nisoli, Few-femtosecond electron transfer dynamics in photoionized donor–π–acceptor molecules, Nat. Chem. (2024), https://doi.org/10.1038/s41557-024-01620-y.
[62] M. Kirsch, H.-G. Korth, V. Stenert, R. Sustmann, H. de Groot, The autoxidation of tetrahydrobiopterin revisited. Proof of superoxide formation from reaction of tetrahydrobiopterin with molecular oxygen, J. Biol. Chem. 278 (2003) 24481–24490, https://doi.org/10.1074/jbc.M211779200.
[63] H. Chosrowjan, S. Taniguchi, N. Mataga, F. Tanaka, A.J.W.G. Visser, The stacked flavin adenine dinucleotide conformation in water is fluorescent on picosecond timescale, Chem. Phys. Lett. 378 (2003) 354–358, https://doi.org/10.1016/S0009-2614(03)01339-3.
[64] S. Niziński, N. Varma, M. Sikorski, T. Tobrman, E. Svobodová, R. Cibulka, M. F. Rode, G. Burdzinski, Fast singlet excited-state deactivation pathway of flavin with a trimethoxyphenyl derivative, Sci. Rep. 14 (2024) 24375, https://doi.org/10.1038/s41598-024-75239-x.